Biophysical Journal
Article

Biophysical Society

A Simulation Study of the Role of Mechanical Stretch in Arrhythmogenesis during Cardiac Alternans

Azzam Hazim,[1] Youssef Belhamadia,[2] and Stevan Dubljevic[3,*]
[1]Department of Biomedical Engineering, University of Alberta, Edmonton, Alberta, Canada; [2]Department of Mathematics and Statistics, American University of Sharjah, Sharjah, United Arab Emirates; and [3]Department of Chemical and Materials Engineering, University of Alberta, Edmonton, Alberta, Canada

ABSTRACT The deformation of the heart tissue due to the contraction can modulate the excitation, a phenomenon referred to as mechanoelectrical feedback (MEF), via stretch-activated channels. The effects of MEF on the electrophysiology at high pacing rates are shown to be proarrhythmic in general. However, more studies need to be done to elucidate the underlying mechanism. In this work, we investigate the effects of MEF on cardiac alternans, which is an alternation in the width of the action potential that typically occurs when the heart is paced at high rates, using a biophysically detailed electromechanical model of cardiac tissue. We observe that the transition from spatially concordant alternans to spatially discordant alternans, which is more arrhythmogenic than concordant alternans, may occur in the presence of MEF and when its strength is sufficiently large. We show that this transition is due to the increase of the dispersion of conduction velocity. In addition, our results also show that the MEF effects, depending on the stretch-activated channels' conductances and reversal potentials, can result in blocking action potential propagation.

SIGNIFICANCE Contraction of the heart muscle affects excitation via stretch-activated channels, a process known as mechanoelectrical feedback (MEF). Previous studies have shown that MEF may play a role in arrhythmogenesis during fast heart rates. However, the underlying mechanisms remain to be elucidated. This study investigates the effects of MEF on electrophysiology during alternans, which is a disturbance in heart rhythm occurring typically at fast rates. We show that stretch can increase the dispersion of conduction velocity, which can induce transition from spatially concordant alternans to spatially discordant alternans, and transition from discordant alternans to conduction failure depending on the stretch-activated channels' conductances and reversal potentials. Our results provide new insights, to our knowledge, into the role of MEF in arrhythmogenesis during alternans.

INTRODUCTION

Irregular excitation waves in the heart may result in cardiac arrhythmias. Ventricular fibrillation (VF) (1,2), which is the most dangerous form of arrhythmias, causes the contraction of the ventricles to become rapid and uncoordinated. It can lead to sudden cardiac death if not treated within minutes. VF is recognized as one of the major causes of death in the industrialized world. Cardiac alternans is characterized by periodic alternations in the action potential (AP) duration (APD) and is believed to precede VF. It can be clinically detected as T-wave alternans using an electrocardiogram and is associated with increased risk of cardiac arrhythmogenesis in many cardiac diseases (3,4).

In a single cell, the APD alternans can be induced by pacing at a sufficiently low basic cycle length (BCL). The genesis of alternans can be described based on APD restitution (5,6). This relation relates the current excited APD with the previous diastolic interval (DI), which is the time between the end of the previous excitation and the current one. The transition from a normal heartbeat to APD alternans occurs when the slope of the APD restitution curve is greater than 1. In cardiac tissue, APD alternans can be spatially concordant (SCA), during which alternation of APD is in phase (whole tissue exhibits the same APD alternation), or discordant (SDA), during which the alternation of APD in

Submitted April 20, 2020, and accepted for publication November 13, 2020.

*Correspondence: stevan.dubljevic@ualberta.ca

Editor: Eric Sobie.

https://doi.org/10.1016/j.bpj.2020.11.018

different regions is out of phase. These discordant regions are separated by a nodal line in which no alternans is present. SDA is considered to be very arrhythmogenic (7,8) because it increases the dispersion of repolarization that can result in blocking AP propagation and initiate reentrant waves. A number of mechanisms have been proposed to explain the production of SDA (see (8–10)). For instance, it has been found that SDA can be formed in tissue when pacing at a sufficiently high rate so that conduction velocity (CV) restitution, i.e., dependency of the speed of the wavefront on the preceding DI, is engaged (9). Also, several dynamic factors such as cardiac memory and calcium cycling dynamics were found to be responsible for the transition from SCA to SDA (see a brief review given in (11)).

It has been shown that cardiac deformation, on the other hand, affects the process of wave propagation via stretch-activated channels (SACs) (12–15). This mechanism is known as mechanoelectrical feedback (MEF). The application of mechanical stretch relative to the different phases of AP can produce different responses depending on the timing and the SACs' conductances and reversal potentials (16–23). Many studies have linked increased mechanical stretch with cardiac arrhythmias (24–30). However, these mechanisms of stretch-induced rhythm disturbances are still not completely understood. Some studies have found that mechanically induced spiral wave breakup, which is a possible mechanism of the VF, may occur as a result of stretch-induced changes in CV (30,31) that can lead to conduction block (CB). Observations on the effects of myocardial stretch on CV have varied widely with respect to cell types, species, experimental preparation, measurement techniques, and mechanical conditions (32). In (33), for instance, the CV in canine Purkinje fiber is initially increased when stretch is increased and then decreased. This has been found not to be the case for the CV in cat trabeculae. The mechanical effects on alternans have been studied from a control point of view in (34–37). In our recent work (38), we showed that the MEF effects on the onset of alternans are antiarrhythmic. It has been demonstrated that the critical BCL (BCL_{crit}), which corresponds to the onset of alternans when MEF is not present, can be shifted to lower values in the presence of MEF. However, only a certain range of BCLs, which are closed to the BCL_{crit}, were considered. As well, a restriction was put on the conductance value of the SACs so that the effects of MEF on the CV can be ignored.

Although studies have shown the effects of stretch on CV and APD restitution properties, a comprehensive study to examine the effects of MEF via SACs with different conductances and reversal potentials on cardiac alternans has not been undertaken, which is the main goal of this article. In this work, we study the effects of MEF on cardiac alternans for different values of reversal potentials and conductances of the SACs using a one-dimensional (1D) realistic electromechanical model of the heart. The underlying mechanisms of the effects of mechanical stretch on the CV and APD properties are described. We find that the increase of the strength of the stretch-activated current (I_{sac}), which is the direct physiological influence of MEF, can increase the spatial dispersion of CV. We show that the increased I_{sac} can increase the spatial repolarization at high pacing rates and discuss the underlying mechanisms. In particular, we explain the role of the increased I_{sac} in the transition from SCA to SDA, and in facilitating CB for some values of the SACs' reversal potentials.

MATERIALS AND METHODS

Electromechanical model of cardiac tissue

The effects of MEF on the dynamics of alternans are studied in this article using a 1D biophysically detailed electromechanical model of cardiac tissue. Mathematically, cardiac excitation and mechanics are described by coupled reaction-diffusion-mechanics system (see (38) for more details). The equations that govern this system can be written as follows:

$$C_m\frac{\partial V}{\partial t}=\frac{D}{F}\frac{\partial}{\partial X}\left(\frac{1}{F}\frac{\partial V}{\partial X}\right)-\left(I_{ion}(\mathbf{u},V)+I_{sac}(\lambda,V)+I_{stim}\right), \tag{1}$$

$$\frac{d\mathbf{u}}{dt}=\mathbf{f}(\mathbf{u},V), \tag{2}$$

$$T_a=h(\mathbf{w}), \tag{3}$$

$$\frac{d\mathbf{w}}{dt}=\mathbf{g}\left(\mathbf{w},\left[Ca^{2+}\right]_i,\lambda,\frac{d\lambda}{dt},T_a\right), \tag{4}$$

$$\frac{\partial}{\partial X}\left(\frac{T_a}{1+\frac{\partial u_d(X)}{\partial X}}+2(c_1+2c_2)\frac{\partial u_d}{\partial X}\right)=0, \tag{5}$$

$$\lambda=F=1+\frac{\partial u_d(X)}{\partial X}, \text{and} \tag{6}$$

$$I_{sac}=G_s\frac{(\lambda-1)}{(\lambda_{max}-1)}(V-E_s). \tag{7}$$

Equations 1 and 2 describe the electrophysiology model, where V is the membrane voltage, C_m is the membrane capacitance, D is the diffusion coefficient, X is a material coordinate, and F is the deformation gradient and is given in Eq. 6. The functions $I_{ion}(\mathbf{u},V)$, $\mathbf{f}(\mathbf{u},V)$, and vector $\mathbf{u}$ are given by Fox et al. model (39), which is an ionic cell model of the canine ventricular myocyte, and I_{stim} is the electrical stimulus. λ is the extension ratio (stretch) and I_{sac} are given by Eqs. 6 and 7, respectively. The excitation-contraction coupling are described by Eqs. 3 and 4, where T_a is the active tension, and the functions $\mathbf{g}$ and h and vector $\mathbf{w}$ are given by the Niederer-Hunter-Smith (NHS) model (40) (see Supporting Material in (38) for a precise form of $\mathbf{w}$, $\mathbf{g}$, and h). $[Ca^{2+}]_i$ is generated by the Fox model. The governing equations for the cardiac mechanics are given by Eq. 5, where $u_d(X)$ is the displacement variable and c_1 and c_2 are the Mooney-Rivlin material (36–38,41)

constants. Finally, λ_{max} is the maximal stretch constant and is given in Eq. 7, and G_s and E_s are the maximal conductance and the reversal potential, respectively, of the SACs.

In this work, the value of G_s is in the range from 0 $\mu S/\mu F$ to 100 $\mu S/\mu F$, and the value of E_s is in the range from -90 to 0 mV (see (38)). The I_{sac} is only present during stretch (i.e., $I_{sac} = 0$ when $\lambda \leq 1$). Equations 1 and 2 are supplemented by no-flux boundary conditions, and Eq. 5. is supplemented with zero displacement boundary conditions modeling an isometric contraction regime. The isometric boundary setting, which was often used in previous cardiac studies (27,29), is used in this study to mimic isovolumic phases in the cardiac cycle. The parameters used in Eqs. 1, 5, and 7 are given in Table 1.

The objective of the article is to study the influence of MEF on the dynamics of alternans using system of Eqs. 1, 2, 3, 4, 5, 6, and 7, denoted here by FOXNHS model. Therefore, this system is solved numerically, and a 7-cm cable of cardiac cells, with both ends fixed, is considered in all simulations. The cable is paced at the boundary or in the middle with different BCLs, and with and without the presence of MEF. All the details about the numerical schemes can be found in (38). The step size $\Delta x = 0.025$ cm and step time $\Delta t = 0.01$ ms were used in all simulations. I_{stim} is applied as square wave pulses with a magnitude of 80 $\mu A/\mu F$ and a duration of 1 ms. Unless otherwise stated, in the presence of MEF, we use values of $G_s = 30$ $\mu S/\mu F$ and $E_s = -10$ mV and vary these parameters to investigate their effects on the alternans. In this work, the amplitude of the alternans is also plotted and is given by

$$a_n(\zeta) = [APD_n(\zeta) - APD_{n-1}(\zeta)](-1)^n, \quad (8)$$

where n and ζ represent the beat number and space, respectively.

RESULTS AND DISCUSSION

The effects of MEF on the APD and CV restitution properties and their role in the transition from SCA to SDA, SDA, and on CB are described in the following four subsections.

Effects of MEF on the APD and CV restitution properties

The FOXNHS model, Eqs. 1, 2, 3, 4, 5, 6, and 7, is first used to study the effects of MEF on APD and CV restitution curves. The APD and CV restitution curves for different values of G_s (Fig. 1) were determined using a dynamic pacing protocol (42). The left panel of Fig. 1 illustrates the APD restitutions obtained by plotting the values of APD, measured at 90% repolarization, against the preceding values of DI for the cell in the middle of the cable using the pacing protocol described in the caption. As can be seen in this figure, MEF changes the APD restitution curve when BCL is greater than 210 ms, which corresponds to a DI close to 60 ms. APD is increasing continuously for a longer BCL; however, after BCL = 210 ms the increase is higher for a larger value of G_s. On the other hand, and for the same values of BCL and G_s, APD decreases when $|E_s|$ is increased, and no effect of MEF on the APD restitution (results not shown) is observed for $|E_s| >= 20$ mV. Note that the effect of MEF on the APD restitution depends on the cell's position within the 1D tissue because the stretching is not uniform along the cable (see (38)). The CV restitutions (*right* of Fig. 1) was constructed by plotting the CV, calculated as the wave propagates from the cell located at 0.5 cm to the cell located at 1 cm from the pacing site (PS), versus the preceding DI. The positions of the cells were selected to avoid boundary effects (43,44). As one can see, CV is monotonically increasing with DI for $G_s < 20$ $\mu S/\mu F$, but it exhibits a biphasic shape when G_s is greater than 20 $\mu S/\mu F$, increasing with BCL till BCL = 300 ms, which corresponds to DI close to 80 ms, then decreasing afterwards.

TABLE 1 Parameter Values Used for the Simulations of the FOXNHS Model

Description	Parameter	Value
Membrane capacitance	C_m	1 μFcm^{-2}
Diffusion	D	$0.001 cm^2 ms^{-1}$
Mooney-Rivlin constant	c_1	0.05 MPa
Mooney-Rivlin constant	c_2	0.025 MPa
Maximal stretch	λ_{max}	1.1

Because the stretch distribution is not uniform along the cable and it varies with BCL (38), the CV depends on the position of the two points in the 1D cable where it is measured. Therefore, we calculated the CV along the cable with and without the presence of MEF for the case when BCL = 300 ms. To this end, we divided the cable, between the positions $X = 0.25$ cm and $X = 6.75$ cm, into 13 segments of equal sizes, then we computed CV between the endpoints of each segment. The measured CV is plotted versus the midpoint of each segment (to the *left* of Fig. 2). As one can see, the change on diffusivity due to stretch when only stretch-dependent conduction is present (MEF is on, set $\lambda = 1$ in I_{sac}), when comparing with the situation in which MEF is off, is decreasing the velocity of propagation of the wave along the cable. However, when only I_{sac} is present (MEF is on, set $\lambda = 1$ in diffusivity), the velocity of propagation of the wave is increased along the cable. It should be noted that although the increase is not monotonic: there is a minimum around $X = 1.5$ cm. When MEF is on, the velocity along the cable is increasing because the increase on CV due to I_{sac} is greater than the decrease on CV because of stretch-dependent conduction. Fig. 2 (*right*) illustrates the effect of the strength of the I_{sac} on CV, for different values of G_s. As can be seen in this figure, CV is decreased, when comparing with the situation in which MEF is off, when $G_s < 20$ $\mu S/\mu F$ and increased when $G_s >= 20$ $\mu S/\mu F$.

To describe the effects of stretch-dependent conduction (when MEF is on and $\lambda = 1$ in I_{sac}) and I_{sac} (when MEF is on and $\lambda = 1$ in diffusivity) on CV, we plotted V, I_{sac}, $D_m = D/F^2 = D/\lambda^2$, and λ simultaneously at steady state for BCL = 300 ms. The result is presented in Fig. 3 for two cells located at different positions. One is located at 1 cm from PS (to the *left* of Fig. 3) and the other one located at 6 cm from PS (to the *right* of Fig. 3). First, the effects of $D_m(\lambda)$ on CV without the presence of I_{sac} is presented in Fig. 3. As can be seen in this figure, λ, at depolarization

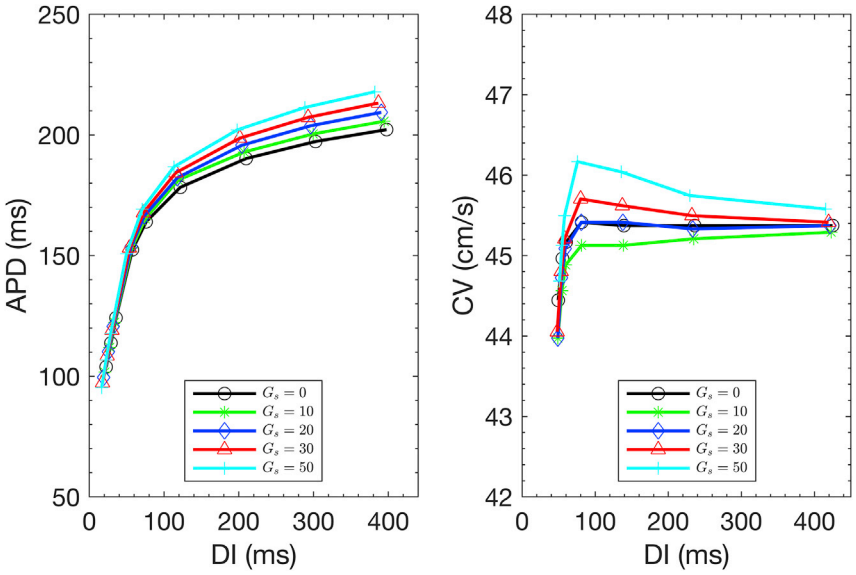

FIGURE 1 (*Left*) Dynamic restitution curves plotting APD against the preceding DI for the middle cell for different values of G_s. For each chosen value of G_s, given in the legend, a 7-cm cable was paced at the middle at an initial BCL of 600 ms for a period of 300 beats. BCL was then reduced by 100 ms and cable was paced for a further 300 beats. This process was repeated but each time BCL, is reduced by 100 ms if it is greater than 300 ms, by 10 ms if it is greater than 250 ms, and by 1 ms if it is greater than 190 ms. APD were plotted versus the preceding DI for seven values of BCL (190, 200, 210, 240, 300, 400, and 600 ms). (*Right*) The CV restitution curves for different values of G_s were determined by plotting CV against the preceding DI. To this end, for each value of G_s, the 1D cable was paced at the boundary using a similar pacing protocol, and the CV was measured at steady state for each BCL as the distance between two points, positioned at 0.5 and 1 cm from the PS, divided by the front arrival times between these points. To see this figure in color, go online.

phase of the AP, is stretching ($\lambda > 1$)), which gives us $D_m(\lambda) < D$; this causes a decrease in the velocity of the wave, and this can also be seen at the left of Fig. 2 (*green dashed lines*) at $X = 1$ cm and $X = 6$ cm. On the other hand, the stretching of cell 2 at the depolarization phase of the AP is higher than the stretching of cell 1. Therefore, the decrease in the velocity of the wave at cell 2 (*right* of Fig. 3; *blue dashed lines*) is higher than the decrease in the velocity of the wave at cell 1 (to the *left* of Fig. 3; *blue dashed lines*). We also need to take into account the decrease of the CV that occurred when the wave propagated from the PS to cell 2.

Fig. 3 illustrates the effects on CV when only I_{sac} is present, as shown in the left panel of Fig. 3. The I_{sac} increases the CV (this can also be seen at $X = 1$ cm at the left of Fig. 2 (*blue dashed lines*)) because at the resting potential and just before the depolarization, the I_{sac}, which is an inward current, slightly increases the resting potential, and this leads to a stronger depolarization effect, causing a preexcitation and an increase of the CV, which corresponds to $X = 6$ cm (to the *left* of Fig. 2; *blue dashed lines*). Note that the increase in CV as shown in Fig. 3 (to the *right*; *red dashed-dotted lines*) that causes an increase in APD is not only due to I_{sac} of the cell 2, but we need also to account

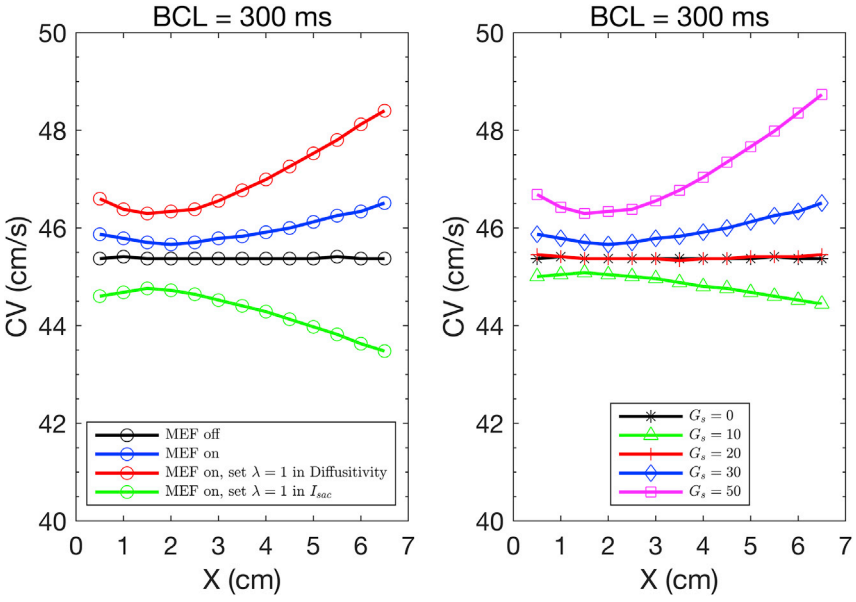

FIGURE 2 CV vs X (distance) along a 7-cm cable, calculated for a BCL of 300 ms under four situations of MEF (*left*) and for different values of G_s (*right*). To see this figure in color, go online.

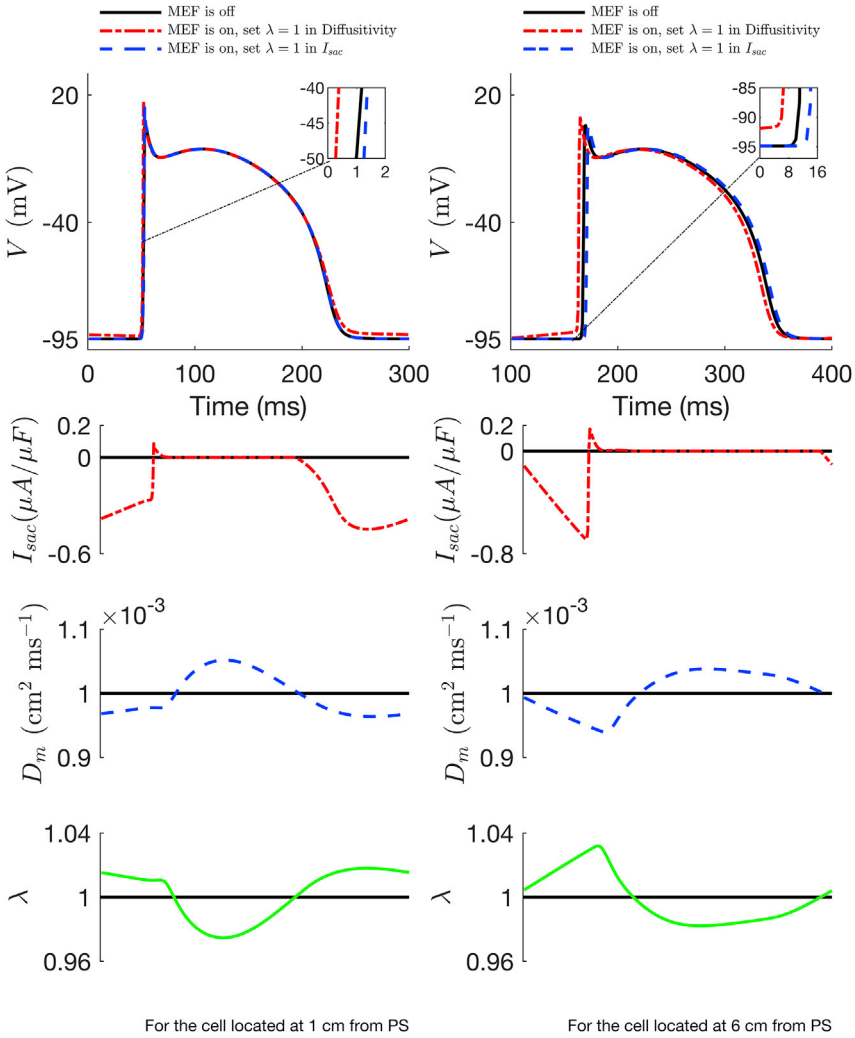

FIGURE 3 Time evolution of V (*top*), I_{sac} (*middle*), D_m (*middle*), and λ (*bottom*) for the cells positioned 1 cm (*left*) and 6 cm (*right*) from the PS, when MEF is off (*black solid lines*) and when MEF is on, and $F = 1$ in the stretch-dependent conduction in Eq. 1. (*red dashed-dotted lines*), and for $G_s = 50\ \mu S/\mu F$, and when MEF is on, and $\lambda = 1$ in I_{sac} (Eq. 7) (*blue dashed lines*) when a 7-cm cable is paced at the boundary with BCL = 400 ms and decreased gradually to BCL = 300 ms, and then paced periodically with BCL = 300 ms until a steady state is reached. To see this figure in color, go online.

for the increase of the CV that occurred when the wave propagates along the cable from the PS to cell 2. At late repolarization, the I_{sac}, which herein is also an inward current, produces a depolarizing effect, slightly delaying the repolarization process. The strength of I_{sac} for the cell 2 (to the *right* of Fig. 3; *red dashed-dotted line*) is larger than the one of the cell 1 (to the *left* of Fig. 3; *red dashed-dotted line*), and therefore, the depolarizing effect of the I_{sac} on the AP of the cell 2 is stronger than the depolarizing effect of the I_{sac} on the AP of the cell 1. At the late repolarization for the case of cell 2, I_{sac} is null because λ is contracting ($\lambda < 1$), and therefore, the I_{sac} has no effect on the AP.

It has been shown in (45,46) as well that an increase in the resting membrane potential has the effect of decreasing the rate of depolarization because of the inactivation of the sodium channels, a process known as accommodation phenomenon that can result in the decrease of CV (30). However, as shown at the right of Fig. 3, the resting potential starts to increase slightly because of the increasing of the strength of the depolarizing I_{sac} ~40 ms before the upstroke of AP, causing an increase of the CV. Therefore, the accommodation effect is insignificant. Similar effects have also been observed by Weise et al. (29) for dynamic stretch-conditions and in (32) for moderate stretch, whereas others have reported a decrease or no change (30,47,48).

For the sake of simplicity, the results in Fig. 3 have been obtained by approximating the diffusion rates of the V (Eq. 1) by moving the term $1/F$ outside the derivative operator so that the effects of deformation on the conductivity and the corresponding diffusion coefficient D can be expressed by $D_m(\lambda)$. This means that a change of the conductivity, due to λ, is assumed to be caused by a dependence on the new diffusion variable D_m on the stretch $(D_m(\lambda))$. This approximation is valid when the term $\partial(1/F)/\partial x$ is small, which is true during alternans. Note that for the FOXNHS model, the onset of alternans occurs at BCL = 206 ms. However, there is error associated with this approximation with BCL = 300 ms. Also, the effects of I_{sac} on CV shown in Fig. 3 for two cells are studied for $G_s = 30\ \mu S/\mu F$. However, increasing G_s, which increases the strength of I_{sac}, has the

effect of increasing CV along the cable (to the *right* of Fig. 2). Therefore, I_{sac} is the dominant factor over the diffusion rates of the V in determining the CV, which may contribute to the formation of an arrhythmic substrate as will be shown in the following sections.

Role of MEF on the transition from SCA to SDA

To illustrate the effect of MEF on the SCA (when, for instance, BCL = 190 ms), two conditions were considered: without and with the presence of MEF. Note that when MEF is not present, the SCA can be induced when pacing at the boundary at a BCL between 187 and 206 ms, and the SDA occurs at a BCL between 178 and 186 ms. For the first condition, a 7-cm cable of cardiac cells was paced at the leftmost boundary, starting at BCL = 400 ms and gradually decreasing to BCL = 190 ms until a steady state was reached. The excited APs travel along the 1D cable in the space-time domain (Fig. 4 *a*; space goes from the *bottom* to the *top* and in time from the *right* to the *left*). As shown in this figure, a large AP is being followed by a small one showing SCA. However, in the presence of MEF (G_s is set to 50 $\mu S/\mu F$) and when similar actions were performed, the SDA rises (Fig. 4 *b*), where the tissue region close to the PS, up to ~2.6 cm and thus showing a pattern of large-short for APDs, whereas the other region showing a pattern of short-large. Fig. 4, *c* and *d* show the spatiotemporal of I_{sac} and λ respectively, under the second condition (i.e., when MEF is present). One can conclude that MEF has a role in converting the SCA into SDA.

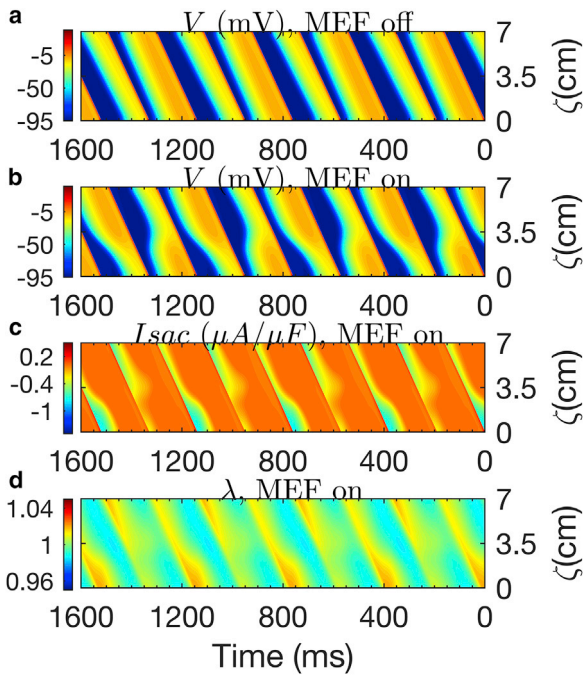

FIGURE 4 Spatiotemporal evolution of V when MEF is off (*a*), when MEF is on (set G_s = 50 $\mu S/\mu F$) (*b*), when MEF is on I_{sac} (*c*), and when MEF is on λ (*d*) for several beats at steady state when a 7-cm cable is paced at the boundary with BCL = 190 ms (starting at BCL = 400 ms and decreased gradually to BCL = 190 ms and then paced periodically with BCL = 190 ms until a steady state is reached). To see this figure in color, go online.

To investigate the role of I_{sac} in this conversion, λ, I_{sac}, and V were plotted simultaneously in Fig. 5 for two cells, namely cell 1 and cell 2, in the cable (cell 1 is located 2 cm from the PS, and cell 2 is located 6 cm from the PS). As shown in this figure, an alternation in the APD induces an alternation in λ (large-small) and, consequently, an alternation in I_{sac} for the same cell in the cable. Therefore, the depolarizing effect of the I_{sac} on the AP is stronger when λ is large, and for the case of cell 1 (*left* of Fig. 5), the increase in the CV for the long APD is greater than for the short APD; however, for the case of cell 2 (*right* of Fig. 5), the increase in the CV for the short APD is greater than for the long APD. Note that although I_{sac} has a slight depolarizing effect on the late repolarization for the long APDs of both cells, the dominant factor is its depolarizing effect at the depolarization phase, and that an increase in the short APD causes, according to the restitution relation, a decrease in the long APD and vice versa. Because the distribution of λ is not uniform along the cable length (Fig. 4 *d*), the effects of I_{sac} (Fig. 4 *c*) on CVs were not equal for all cardiac cells along the cable.

To illustrate the variation of APD with CV along the 1D tissue, the CVs and APDs for two consecutive beats at steady state were plotted simultaneously in Fig. 6. When MEF is not present, an SCA is formed, which corresponds to an oscillation of large and short APDs that are correlated respectively with greater and smaller CVs. However, when MEF is present, a transition from SCA to SDA is induced, which is mainly due to the effect of I_{sac} via its influence on the CV. As shown in Fig. 6 (*top*), when the two dot-dashed lines intersect at a point (called nodal point and is located at ~2.6 cm from the PS), the long and short APDs become equal, and this marks the division of two out-of-phase regions. Fig. 7 illustrates the effects of the strength of I_{sac}, which can be regulated by the value of G_s, on the position of the nodal point. Therefore, increased I_{sac} may play a role for facilitating the transition from SCA to SDA. With varied levels of the increase in the strength of I_{sac}, SDA was observed with the nodes, formed in the presence of MEF, moved toward the PS in response to an increase in G_s, suggesting susceptibility of the tissue to genesis of SDA.

Depending on the BCL applied, the strength of I_{sac} that is required to cause a transition from SCA to SDA varies (see Fig. 8). As shown in this figure, one can observe that G_s decreases monotonically when BCL decreases from 204 to 187 ms for the transition from SCA to SDA to occur. However, for the cases (BCL = 206 ms, $G_s \geq 50$ $\mu S/\mu F$) and (BCL = 205 ms, $G_s \geq 55$ $\mu S/\mu F$), no alternans occurred. This was because when MEF is off, the $|a_n(\zeta)|$ at these BCLs were relatively small and for large values of G_s, the strength of the I_{sac} was large enough to suppress alternans.

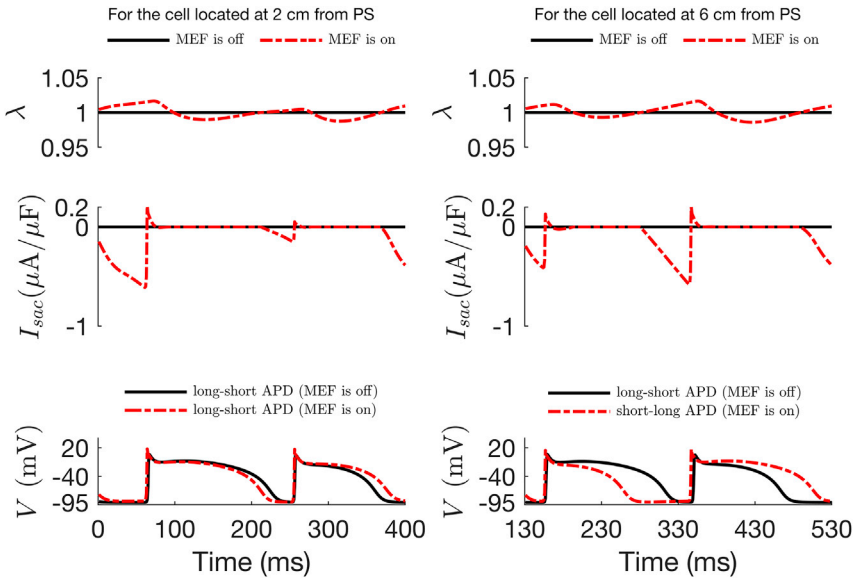

FIGURE 5 Time evolution of V (*bottom*), I_{sac} (*middle*), and λ (*top*) for the cells positioned 2 cm (*left*) and 6 cm (*right*) from the PS for $G_s = 0\ \mu S/\mu F$ (MEF is off; *black solid line*) and for $G_s = 50\ \mu S/\mu F$ (MEF is on; *red dashed-dotted line*) when a 7-cm cable is paced at the boundary with BCL = 400 ms and decreased gradually to BCL = 190 ms and then paced periodically with BCL = 190 ms until a steady state is reached. To see this figure in color, go online.

This is similar to what was observed for LR1NHS, in our previous study (38), in which the Luo-Rudy phase one model (49) was used to represent the electrical activity. There, we showed that, for a certain range of BCLs close to the alternans bifurcation, MEF has the effect of suppressing alternans.

Role of MEF on SDA

Similar to what we did in the previous section, the effect of MEF on the SCA is illustrated here when, for instance, BCL = 180 ms. The V, λ, and I_{sac} at steady state and under the two conditions were plotted simultaneously in Fig. 9. As

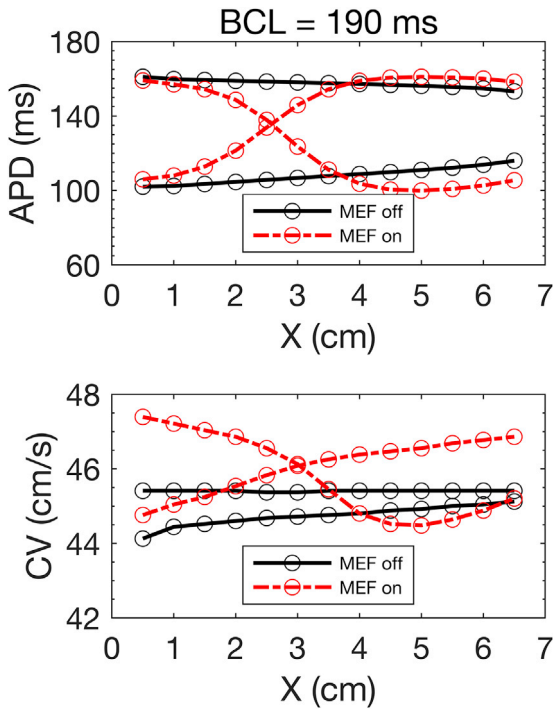

FIGURE 6 APDs (*top*) and CVs (*bottom*) vs X (distance) along a 7-cm cable for the same two consecutive beats at steady state calculated for a BCL of 190 ms and when MEF is off (*black solid lines*) and MEF is on (*red dashed-dotted lines*). To see this figure in color, go online.

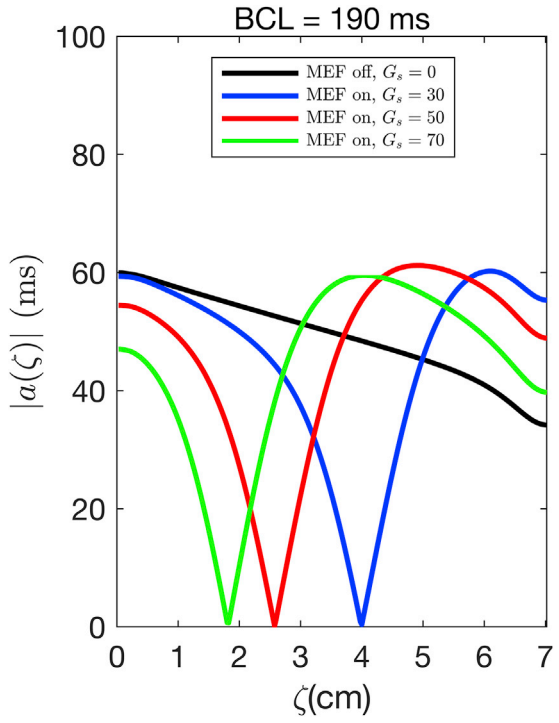

FIGURE 7 Magnitude of the amplitude of alternans at steady state for different values of G_s, when a 7-cm cable is paced at the boundary with BCL = 400 ms and decreased gradually to BCL = 190 ms, and then paced periodically with BCL = 190 ms. APD at 90% repolarization was adopted as a measure of APD. To see this figure in color, go online.

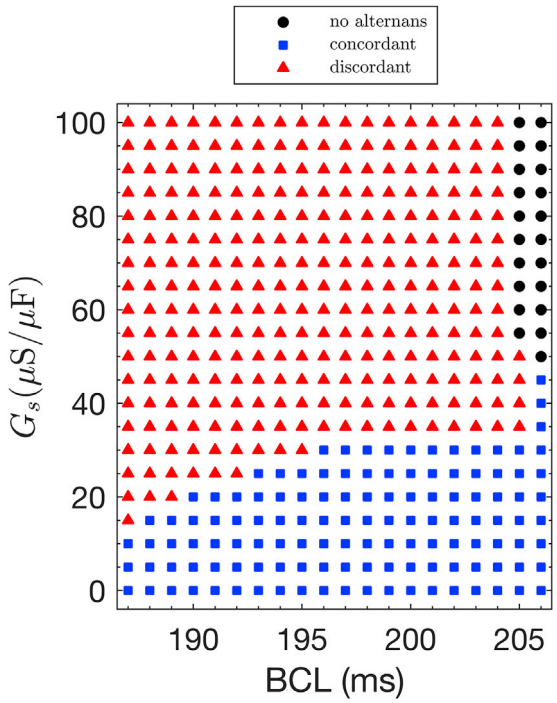

FIGURE 8 Plot showing the different patterns of alternans that are formed because of the I_{sac} in the plane of G_s and BCL when a 7-cm cable is paced at the boundary with BCL = 400 ms and decreased gradually to a BCL in the range of 187–206 ms until a steady state is reached. As shown, the formed patterns are no alternans (*black circles*), concordant alternans (*blue squares*), and discordant alternans (*red triangles*). To see this figure in color, go online.

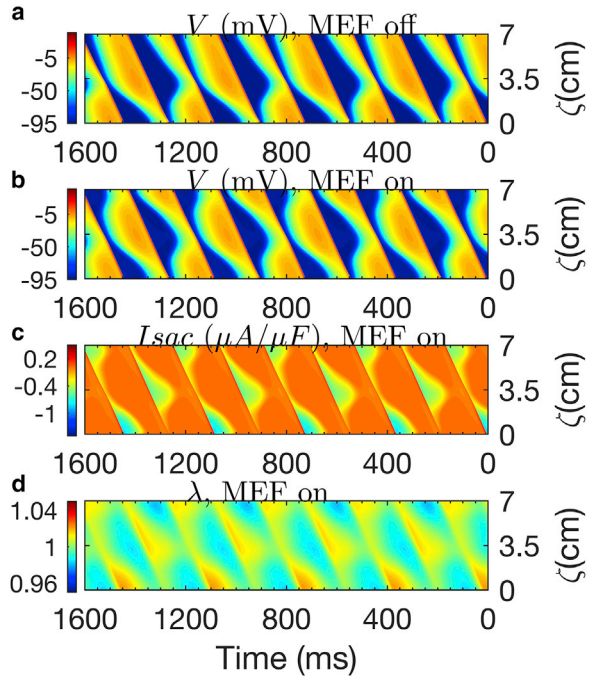

FIGURE 9 Spatiotemporal evolution of V when MEF is off (*a*), MEF is on (*b*), MEF is on I_{sac} (*c*), and when MEF is on λ (*d*) for $G_s = 50\ \mu S/\mu F$ and for several beats at steady state when a 7-cm cable is paced at the boundary with BCL = 180 ms (starting at BCL = 400 ms and decreased gradually to BCL = 180 ms). To see this figure in color, go online.

shown in Fig. 9 *b*, the spatial dispersion of repolarization was increased in the presence of MEF (G_s is set to 50 μS/μF) when compared to alternans repolarization without the presence of MEF (Fig. 9 *a*). As shown in this figure, the SDA has a nodal point formed at ~2 cm from the PS, where the alternation of APDs in the region of the cable from the PS to this nodal point is manifested as a long-short, whereas the alternation of the APDs in the region after this point is manifested as a short-long pattern. One can also see that in the presence of MEF (Fig. 9 *b*), the number of nodal points (two nodes were formed) was increased where the second node was formed at ~5.8 cm from the PS. In Fig. 9 *b*, the APDs alternate as a pattern of short-long in the region between the two nodes and as a pattern of long-short in other regions (one from the PS up to ~2 cm and the other from ~5.8 cm to the end of the cable).

Fig. 10 illustrates the variation of APD with CV for two consecutive beats at steady state. As shown in this figure, the CV was increased globally, when compared with the one without MEF, for both short and long APDs along the cable up to ~5.4 cm from the PS. Because of I_{sac}, the CV of large (small) APD is decreasing (increasing) in the cable from the PS up to the first node located at ~2 cm from the PS. This node almost coincides with the one that is formed when MEF is not present. The previously long (short) APD becomes short (long) APD between the first and the second node located at ~5.8 cm from the PS. Between these nodes, the CV of long (short) is increasing (decreasing) until approximately the middle of the cable, then decreasing (increasing) till the second node. The CV of the small APD starts to increase significantly after the AP travels 5 cm from the PS. Consequently, the small APD starts to increase significantly and causes the long APD to decrease according to the restitution relation until the second node is formed at ~5.8 cm from the PS.

The strength of I_{sac}, by varying the G_s, affects the formation of the nodes and their positions (Fig. 11). As shown in this figure, for $G_s = 30\ \mu S/\mu F$, no additional nodes are formed to the already existing node when MEF is not present. However, for the values of G_s equal to 50 μS/μF or 70 μS/μF, a second node is formed closer to the other end of the cable and moves more toward the PS when G_s is greater. It has been shown in (10,50) that if a cable is paced at one end with low BCL, then SDA nodes tend to form at the other end of the cable and move toward the paced end in response to a decrease in BCL. This suggested that an increased G_s may facilitate the genesis of SDA. Although the degree of APD oscillation is greater when MEF is applied, the magnitude of the amplitude of alternans is decreased. As shown in Fig. 11, the additional node is formed at ~5.8 cm from the PS. However, in Fig. 10, it is shown that it is formed at ~5.6 cm. This difference is due

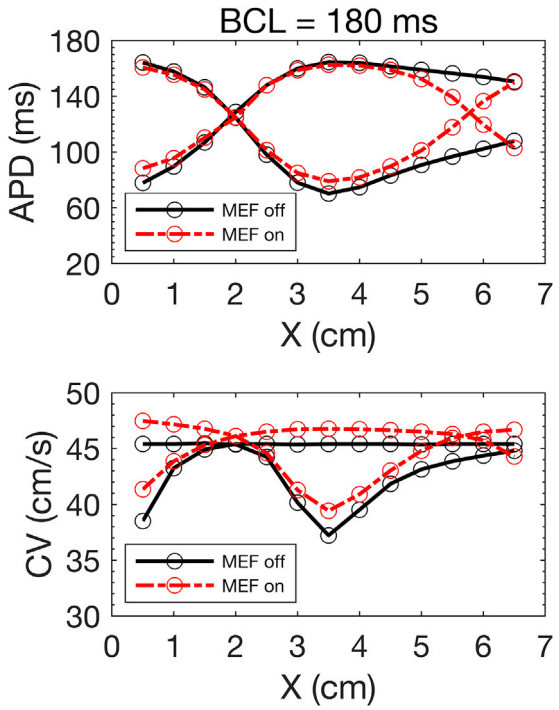

FIGURE 10 APDs (*top*) and CVs (*bottom*) vs X (distance) along a 7-cm cable, for the same two consecutive beats at steady state, calculated for a BCL of 180 ms and when MEF is off (*black solid lines*) and MEF is on (*red dashed-dotted lines*). To see this figure in color, go online.

to the accumulation of errors accrued along all segments in which the CVs were computed because the distance between the two points of a segment in which the CV was computed is not small enough so that the local error remains small.

Role of MEF on CB

To investigate the role of MEF on the threshold of CB, we performed the following steps. First, we determined the CB threshold without the presence of MEF. Thus, the 1D cable was paced at the boundary, when MEF is off, using the same pacing protocol described above but with BCL = 200 ms. If CB did not occur, the same operation was repeated but every time, BCL was decreased 1 ms until CB occurred. The CB was observed when BCL = $\text{BCL}_{\text{thresMEFoff}} = 177$ ms, where $\text{BCL}_{\text{thresMEFoff}}$ is the smallest BCL under which CB occurred for this model when MEF was not present.

In the presence of MEF, the same steps were repeated for three different settings of E_s (namely $E_s = 0$, -10, and -20 mV) of the I_{sac}. For every setting of E_s, different values of G_s, between 0 and 100 μS/μF, were also considered. We observed that only when $E_s = 0$ mV and for $G_s > = 80$ μS/μF, the threshold of CB was shifted 3 ms to higher BCLs; this means that BCL = $\text{BCL}_{\text{thresMEFon}} = 180$ ms, where $\text{BCL}_{\text{thresMEFon}}$ is the smallest BCL under which CB occurred when MEF was present. As shown in Fig. 12 *Ab*, CB occurred when the wave front, marked by the red star, of the 62nd stimulus (beat no. 62), initiated at time $t_1 = 19{,}060$ ms, hits the tail of the preceding wave, causing CB of the propagating AP. At steady state, a conduction of the even beats can no longer be sustained (Fig. 12 *Bb*), and a CB always occurred at the vicinity of the PS and, therefore, was predisposed to a higher risk of arrhythmogenesis. These results suggested that the value of parameter E_s of the I_{sac} plays an important role in the conduction of AP that may result in the transition from SDA to conduction failure.

The effect of E_s on the variation of I_{sac}, and consequently on the AP CV, can be described as follows. In one direction, changing E_s can change the magnitude and sign (inward or outward) of the I_{sac}, which can have an effect on the APDs. In the other direction, variations in the APDs can change the λ, and this, in turn, can modify the I_{sac}. As an illustration, λ, I_{sac}, and V were plotted simultaneously at intermediate states (beat numbers 60 and 61 corresponding to BCL = 180 ms) for the cell located at 2 cm from the PS and for $E_s = 0$ mV and $E_s = -10$ mV (*left* and *right* of Fig. 13, respectively). As one can see, the variations of λ are not same. Therefore, the magnitudes and signs of I_{sac} are also not the same for these values. At beat number 60, the magnitude of the I_{sac}, which is an inward current before the depolarization phase (to the *left* of Fig. 13; the case of

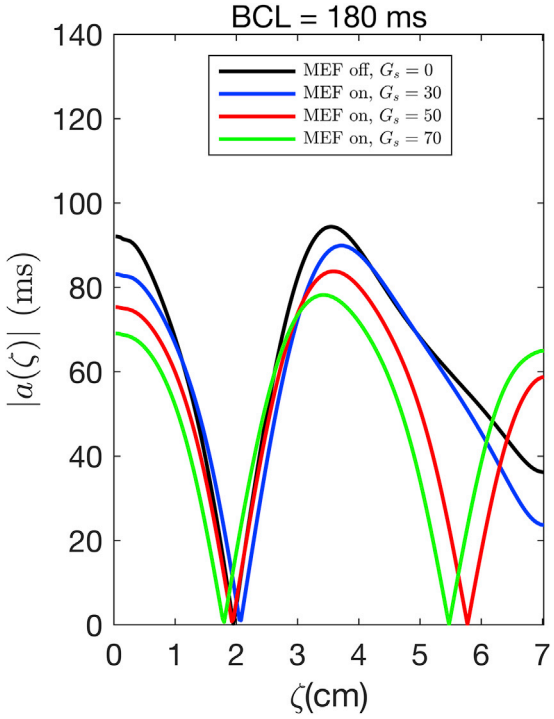

FIGURE 11 Magnitude of the amplitude of alternans at steady state for different values of G_s when a 7-cm cable is paced at the boundary with BCL = 400 ms and decreased gradually to BCL = 180 ms and then paced periodically with BCL = 180 ms. APD at 90% repolarization was adopted as a measure of APD. To see this figure in color, go online.

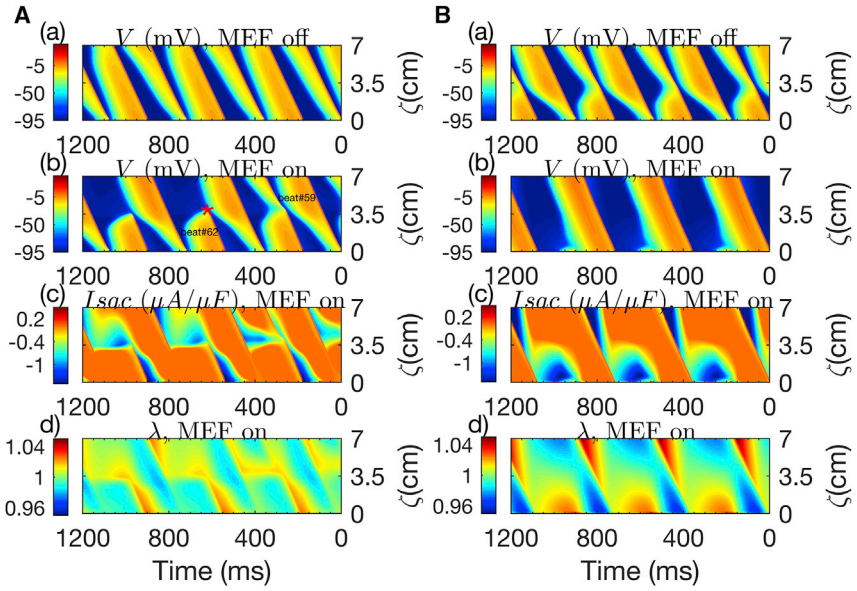

FIGURE 12 Spatiotemporal evolution of V when MEF is off (*a*), and on (*b*), I_{sac} (*c*), λ (*d*) for $E_s = 0$ ms and $G_s = 80\ \mu S/\mu F$ for several beats at intermediate states (*A*) and steady states (*B*), when a 7-cm cable is paced at the boundary, starting at BCL = 400 ms, and decreased gradually to BCL = 180 ms. (*Ab*) The wave front (*red star*) of the 62nd beat (beat no. 62) hits the refractory tail of the preceding wave. (*Bb*) The waves of the even paced beats collide with the preceding waves of the odd beats at the vicinity of PS. To see this figure in color, go online.

$E_s = 0$ mV), is larger than the one shown at the right panel of Fig. 13 (the case of $E_s = -10$ mV), and at early repolarization, I_{sac} was an outward current and became an inward current for the case of $E_s = 0$ mV, whereas for the case of $E_s = -10$ mV, it became about zero. However, at beat number 61, and before the depolarization, I_{sac} was zero for $E_s = 0$ mV, whereas for $E_s = -10$ mV, it was not. On the other hand, it was shown that the I_{sac} magnitude, sign, and timing play a significant role in the dispersion of repolarization via its influence on the CV dispersion.

The effect of E_s on the dispersion of CVs for the 5th, 40th, 52nd, 60th, and 61st beats is illustrated in Fig. 14. As can be seen in this figure, the CVs along the cable for the beat number five corresponding to BCL = 390 ms (*top left* of Fig. 14), the beat number 40 corresponding to BCL = 197 ms (*top right* of Fig. 14), and the beat number 52 corresponding to BCL = 185 ms (*bottom left* of Fig. 14) were changed for $E_s = 0$ mV, when compared with $E_s = -10$ mV. Large oscillations on the CV, when $E_s = 0$ mV, $E_s = -10$ mV, and $E_s = -20$ mV, were observed from the 61st beat corresponding to BCL = 180 ms (*bottom right* of Fig. 14), during which the CV for the case of $E_s = 0$ mV was relatively increased, when compared to $E_s = -10$ mV, leading to CB at the successive beats starting

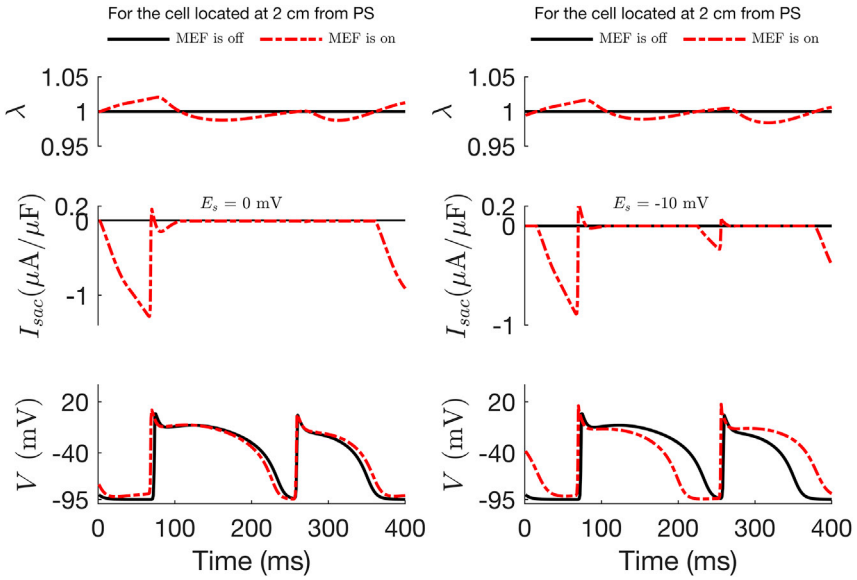

FIGURE 13 Time evolution of V (*bottom*), I_{sac} (*middle*), and λ (*top*) for the cell positioned 2 cm from the PS for $G_s = 80\ \mu S/\mu F$ and $E_s = 0$ mV (*left*) and $E_s = -10$ mV (*right*) when a 7-cm cable is paced at the boundary with BCL = 400 ms and decreased gradually to BCL = 180 ms. Only the corresponding V, I_{sac}, and λ for the beats 60 and 61 are illustrated. To see this figure in color, go online.

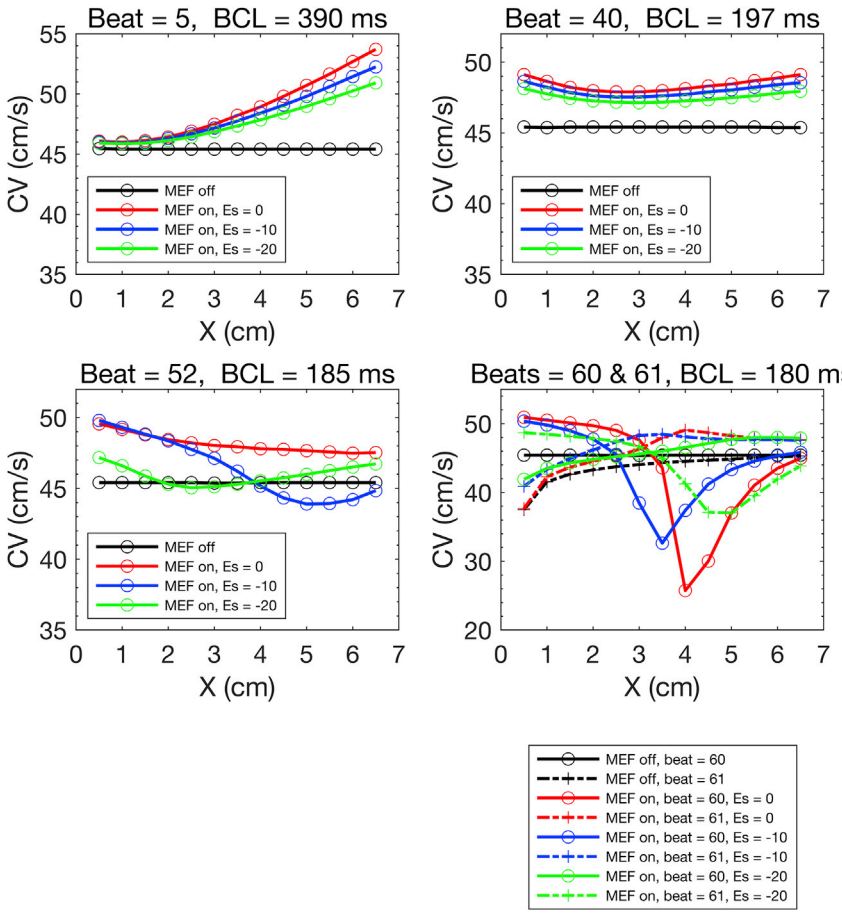

FIGURE 14 CV vs X along a 7-cm cable when MEF is off and MEF is on (with $G_s = 80\ \mu S/\mu F$ and for three different values of E_s, which are 0, -10, and -20 mV), calculated at beat numbers 5 (*top left*), 40 (*top right*), 52 (*bottom left*), 60 and 61 (*bottom right*). To see this figure in color, go online.

at beat number 62. However, for the case of $E_s = -20$ mV, the CV was relatively decreased. These findings suggest that myocardial stretch can increase the dispersion of CV, depending on BCL, G_s, and E_s of the SACs and that the increase that was enhanced at short BCL altered direction of wave propagation and increased occurrence of local CB.

CONCLUSIONS

We investigated the effects of MEF delivered via SACs on the dynamics of alternans using a 1D biophysically detailed electromechanical model of cardiac tissue. Numerical simulations were performed for a range of pacing periods and for different values of the SACs' conductances and reversal potentials. We demonstrated that MEF at high pacing rates is associated with an increased risk of arrhythmogenesis because it can increase the dispersion of repolarization and refractoriness via its influence on the CV. In particular, we showed that MEF may increase spatial dispersion of CV along the 1D tissue during alternans and might facilitate the genesis of SDA and conduction failure, depending on the SACs' reversal potentials and conductances. For two-dimensional and three-dimensional cardiac tissue, the SDA has been shown to induce the formation of reentrant waves, and this may break down further, leading to multiple wavelets corresponding to the onset of lethal arrhythmias such as VF. Therefore, studying the mechanisms underlying the transition from SDA into a reentry wave due to MEF and how this further evolves into lethal cardiac arrhythmias is of great interest and may be addressed in future studies. It has been also shown that hypothermia of short duration could annihilate the spiral wave breakup (51). Therefore, studying the effect of coupling MEF-heat on reentrant waves is also important. This will be the subject of future work as well.

AUTHOR CONTRIBUTIONS

A.H. designed the research, performed and analyzed the simulations, and wrote the manuscript. Y.B. and S.D. contributed to the study design, funding acquisition, review, editing, and provided critical feedback.

ACKNOWLEDGMENTS

The authors thank the Natural Sciences and Engineering Research Council of Canada for financial support. The second author gratefully acknowledges an American University of Sharjah Enhanced Faculty Research Grant. The work in this article was supported, in part, by the Open Access Program from the American University of Sharjah.

REFERENCES

1. Makarov, L., and V. Komoliatova. 2010. Microvolt T-wave alternans during Holter monitoring in children and adolescents. *Ann. Noninvasive Electrocardiol.* 15:138–144.
2. Narayan, S. M. 2007. T-wave alternans and human ventricular arrhythmias: what is the link? *J. Am. Coll. Cardiol.* 49:347–349.
3. Giudici, M. C., and M. P. Savage. 1990. Transient pulsus alternans during acute myocardial ischemia and its resolution following beta-adrenergic blockade. *Am. Heart J.* 119:960–962.
4. Kroll, C. R., and L. S. Gettes. 2002. T wave alternans and Torsades de Pointes after the use of intravenous pentamidine. *J. Cardiovasc. Electrophysiol.* 13:936–938.
5. Nolasco, J. B., and R. W. Dahlen. 1968. A graphic method for the study of alternation in cardiac action potentials. *J. Appl. Physiol.* 25:191–196.
6. Guevara, M. R., G. Ward, …, L. Glass. 1984. Electrical alternans and period doubling bifurcations. *IEEE Comp. Cardiol.* 562:167–170.
7. Rubenstein, D. S., and S. L. Lipsius. 1995. Premature beats elicit a phase reversal of mechanoelectrical alternans in cat ventricular myocytes. A possible mechanism for reentrant arrhythmias. *Circulation.* 91:201–214.
8. Pastore, J. M., S. D. Girouard, …, D. S. Rosenbaum. 1999. Mechanism linking T-wave alternans to the genesis of cardiac fibrillation. *Circulation.* 99:1385–1394.
9. Qu, Z., A. Garfinkel, …, J. N. Weiss. 2000. Mechanisms of discordant alternans and induction of reentry in simulated cardiac tissue. *Circulation.* 102:1664–1670.
10. Watanabe, M. A., F. H. Fenton, …, A. Karma. 2001. Mechanisms for discordant alternans. *J. Cardiovasc. Electrophysiol.* 12:196–206.
11. Tse, G., S. T. Wong, …, J. M. Yeo. 2016. Cardiac dynamics: alternans and arrhythmogenesis. *J. Arrhythm.* 32:411–417.
12. Lab, M. J. 1996. Mechanoelectric feedback (transduction) in heart: concepts and implications. *Cardiovasc. Res.* 32:3–14.
13. Kohl, P., P. Hunter, and D. Noble. 1999. Stretch-induced changes in heart rate and rhythm: clinical observations, experiments and mathematical models. *Prog. Biophys. Mol. Biol.* 71:91–138.
14. Kohl, P., and U. Ravens. 2003. Cardiac mechano-electric feedback: past, present, and prospect. *Prog. Biophys. Mol. Biol.* 82:3–9.
15. Quinn, T. A., P. Kohl, and U. Ravens. 2014. Cardiac mechano-electric coupling research: fifty years of progress and scientific innovation. *Prog. Biophys. Mol. Biol.* 115:71–75.
16. White, E., J. Y. Le Guennec, …, D. Garnier. 1993. The effects of increasing cell length on auxotonic contractions; membrane potential and intracellular calcium transients in single Guinea-pig ventricular myocytes. *Exp. Physiol.* 78:65–78.
17. Hu, H., and F. Sachs. 1997. Stretch-activated ion channels in the heart. *J. Mol. Cell. Cardiol.* 29:1511–1523.
18. Zeng, T., G. C. Bett, and F. Sachs. 2000. Stretch-activated whole cell currents in adult rat cardiac myocytes. *Am. J. Physiol. Heart Circ. Physiol.* 278:H548–H557.
19. Kelly, D., L. Mackenzie, …, D. A. Saint. 2006. Gene expression of stretch-activated channels and mechanoelectric feedback in the heart. *Clin. Exp. Pharmacol. Physiol.* 33:642–648.
20. Garny, A., and P. Kohl. 2004. Mechanical induction of arrhythmias during ventricular repolarization: modeling cellular mechanisms and their interaction in two dimensions. *Ann. N. Y. Acad. Sci.* 1015:133–143.
21. Li, W., P. Kohl, and N. Trayanova. 2004. Induction of ventricular arrhythmias following mechanical impact: a simulation study in 3D. *J. Mol. Histol.* 35:679–686.
22. Kohl, P., C. Bollensdorff, and A. Garny. 2006. Effects of mechanosensitive ion channels on ventricular electrophysiology: experimental and theoretical models. *Exp. Physiol.* 91:307–321.
23. Kohl, P., F. Sachs, and M. R. Franz. 2011. Cardiac Mechano-Electric Coupling and Arrhythmias. Oxford University Press, Oxford.
24. Kohl, P., A. D. Nesbitt, …, M. Lei. 2001. Sudden cardiac death by Commotio cordis: role of mechano-electric feedback. *Cardiovasc. Res.* 50:280–289.
25. Bierfeld, J. L., V. Rodriguez-Viera, …, B. Befeler. 1979. Terminating ventricular fibrillation by chest thump. *Angiology.* 30:703–707.
26. Li, W., P. Kohl, and N. Trayanova. 2006. Myocardial ischemia lowers precordial thump efficacy: an inquiry into mechanisms using three-dimensional simulations. *Heart Rhythm.* 3:179–186.
27. Panfilov, A. V., R. H. Keldermann, and M. P. Nash. 2007. Drift and breakup of spiral waves in reaction-diffusion-mechanics systems. *Proc. Natl. Acad. Sci. USA.* 104:7922–7926.
28. Keldermann, R. H., M. P. Nash, …, A. V. Panfilov. 2010. Electromechanical wavebreak in a model of the human left ventricle. *Am. J. Physiol. Heart Circ. Physiol.* 299:H134–H143.
29. Weise, L. D., and A. V. Panfilov. 2013. A discrete electromechanical model for human cardiac tissue: effects of stretch-activated currents and stretch conditions on restitution properties and spiral wave dynamics. *PLoS One.* 8:e59317.
30. Hu, Y., V. Gurev, …, N. A. Trayanova. 2013. Effects of mechano-electric feedback on scroll wave stability in human ventricular fibrillation. *PLoS One.* 8:e60287.
31. Weise, L. D., and A. V. Panfilov. 2017. Mechanism for mechanical wave break in the heart muscle. *Phys. Rev. Lett.* 119:108101.
32. McNary, T. G., K. Sohn, …, F. B. Sachse. 2008. Experimental and computational studies of strain-conduction velocity relationships in cardiac tissue. *Prog. Biophys. Mol. Biol.* 97:383–400.
33. Rosen, M. R., M. J. Legato, and R. M. Weiss. 1981. Developmental changes in impulse conduction in the canine heart. *Am. J. Physiol.* 240:H546–H554.
34. Deshpande, D., Y. Belhamadia, and S. Dubljevic. 2011. Cardiac alternans annihilation by distributed mechano-electric feedback (MEF). *Annu. Int. Conf. IEEE Eng. Med. Biol. Soc.* 2011:259–262.
35. Yapari, F., D. Deshpande, …, S. Dubljevic. 2014. Control of cardiac alternans by mechanical and electrical feedback. *Phys. Rev. E Stat. Nonlin. Soft Matter Phys.* 90:012706.
36. Hazim, A., Y. Belhamadia, and S. Dubljevic. 2015. Control of cardiac alternans in an electromechanical model of cardiac tissue. *Comput. Biol. Med.* 63:108–117.
37. Hazim, A., Y. Belhamadia, and S. Dubljevic. 2018. Mechanical perturbation control of cardiac alternans. *Phys. Rev. E.* 97:052407.
38. Hazim, A., Y. Belhamadia, and S. Dubljevic. 2019. Effects of mechano-electrical feedback on the onset of alternans: a computational study. *Chaos.* 29:063126.
39. Fox, J. J., J. L. McHarg, and R. F. Gilmour, Jr. 2002. Ionic mechanism of electrical alternans. *Am. J. Physiol. Heart Circ. Physiol.* 282:H516–H530.
40. Niederer, S. A., P. J. Hunter, and N. P. Smith. 2006. A quantitative analysis of cardiac myocyte relaxation: a simulation study. *Biophys. J.* 90:1697–1722.
41. Nash, M. P., and A. V. Panfilov. 2004. Electromechanical model of excitable tissue to study reentrant cardiac arrhythmias. *Prog. Biophys. Mol. Biol.* 85:501–522.
42. Koller, M. L., M. L. Riccio, and R. F. Gilmour, Jr. 1998. Dynamic restitution of action potential duration during electrical alternans and ventricular fibrillation. *Am. J. Physiol.* 275:H1635–H1642.
43. Cherry, E. M., and F. H. Fenton. 2011. Effects of boundaries and geometry on the spatial distribution of action potential duration in cardiac tissue. *J. Theor. Biol.* 285:164–176.
44. Kelly, A., I. A. Ghouri, …, G. L. Smith. 2013. Subepicardial action potential characteristics are a function of depth and activation sequence in isolated rabbit hearts. *Circ. Arrhythm. Electrophysiol.* 6:809–817.
45. Hodgkin, A. L., and A. F. Huxley. 1952. A quantitative description of membrane current and its application to conduction and excitation in nerve. *J. Physiol.* 117:500–544.

46. Biktashev, V. N. 2002. Dissipation of the excitation wave fronts. *Phys. Rev. Lett.* 89:168102.

47. Zhu, W.-X., S. B. Johnson, …, D. L. Packer. 1997. Impact of volume loading and load reduction on ventricular refractoriness and conduction properties in canine congestive heart failure. *J. Am. Coll. Cardiol.* 30:825–833.

48. Walters, T. E., G. Lee, …, J. M. Kalman. 2014. Acute atrial stretch results in conduction slowing and complex signals at the pulmonary vein to left atrial junction: insights into the mechanism of pulmonary vein arrhythmogenesis. *Circ. Arrhythm. Electrophysiol.* 7:1189–1197.

49. Luo, C. H., and Y. Rudy. 1991. A model of the ventricular cardiac action potential. Depolarization, repolarization, and their interaction. *Circ. Res.* 68:1501–1526.

50. Echebarria, B., and A. Karma. 2007. Amplitude equation approach to spatiotemporal dynamics of cardiac alternans. *Phys. Rev. E Stat. Nonlin. Soft Matter Phys.* 76:051911.

51. Belhamadia, Y., and J. Grenier. 2019. Modeling and simulation of hypothermia effects on cardiac electrical dynamics. *PLoS One.* 14:e0216058.